Radiological and leaching assessment of an ettringite-based mortar from ladle slag and phosphogypsum

Peer-reviewed author version

GIJBELS, Katrijn; Nguyen, Hoang; Kinnunen, Paivo; SAMYN, Pieter; SCHROEYERS, Wouter; Pontikes, Yiannis; SCHREURS, Sonja & Illikainen, Mirja
(2020) Radiological and leaching assessment of an ettringite-based mortar from ladle slag and phosphogypsum. In: Cement and Concrete Research, 128 (Art N° 105954).

DOI: 10.1016/j.cemconres.2019.105954
Handle: http://hdl.handle.net/1942/30092

RADIOLOGICAL AND LEACHING ASSESSMENT OF AN ETTRINGITE-BASED MORTAR FROM LADLE SLAG AND PHOSPHOGYPSUM

Katrijn GIJBELS[a*], Hoang NGUYEN[b], Paivo KINNUNEN[b], Pieter SAMYN[c], Wouter SCHROEYERS[a], Yiannis PONTIKES[d], Sonja SCHREURS[a], Mirja ILLIKAINEN[b]

[a] Hasselt University, CMK, Nuclear Technological Centre, Agoralaan, Gebouw H, 3590 Diepenbeek, Belgium

[b] Fibre and Particle Engineering Research Unit, University of Oulu, Pentti Kaiteran katu 1, 90014 Oulu, Finland

[c] Hasselt University, IMO, Applied and Analytical Chemistry, Agoralaan, Gebouw D, 3590 Diepenbeek, Belgium

[d] KU Leuven, Department of Materials Engineering, Kasteelpark Arenberg 44, 3001 Leuven, Belgium

* Corresponding author: Katrijn GIJBELS

katrijn.gijbels@uhasselt.be, hoang.nguyen@oulu.fi, paivo.kinnunen@oulu.fi, pieter.samyn@uhasselt.be, wouter.schroeyers@uhasselt.be, yiannis.pontikes@kuleuven.be, sonja.schreurs@uhasselt.be, mirja.illikainen@oulu.fi

Declarations of interest: none

Abstract

In this investigation, ettringite-based mortars were synthesized from ladle slag (LS) and phosphogypsum (PG), promoting the concept of a circular economy. However, the reuse of naturally occurring radioactive materials (NORM), such as PG, requires radiological investigation. Also, the immobilization degree for contaminants contained in PG should be evaluated. The former was investigated using gamma spectroscopy and radon exhalation/emanation tests, while the latter was assessed using an up-flow percolation column test according to the CEN/TS 16637-3. The produced mortars comply with current legislation on naturally occurring radionuclides (NOR) in building materials, proving that they can be safely used for building purposes. The radon emanation decreased upon increasing the Polish PG content, which was mainly determined by the microporosity. The specific surface areas were 20-30 times lower than conventional cement, and the immobilization degree for contaminants was generally high (> 90%). This investigation demonstrates high potential for PG reuse in ettringite-based mortars.

Keywords

Ladle slag, phosphogypsum, ettringite, naturally occurring radionuclides, leaching

1. Introduction

In the development of a more sustainable construction industry, many research efforts are focused on the partial or even total replacement of Ordinary Portland Cement (OPC) content with by-products [1], for example, slags [2,3]. One such by-product is ladle slag (LS) from the steel-making process [4,5]. Unlike other slags, LS has gained much less attention due to its crystallinity and free CaO content. About 80% of LS generated in Europe is landfilled or stored [5], which amounts to roughly 1.5-1.9 million tons annually. However, the feasibility of

LS for the production of cementitious materials has been advocated in the literature, e.g. as a sole precursor in alkali-activated pastes [6], mortars [7] and composites [8], with promising mechanical properties.

LS can also effectively be used for the synthesis of ettringite-based binders from its hydration with gypsum and water [9–11]. Generally, ettringite-based binders show rapid strength gain and are compatible with conventional cementitious matrices [12]. Since alkali silicates and hydroxides cannot be sourced naturally, their production involves costs and energy usage, significantly contributing to the environmental footprint of alkali-activated binders [13]. Therefore, ettringite-based binders, which do not require alkali activation, are very promising materials from both an economical and sustainability perspective. Further, the abundance of various types of gypsum waste shows the potential for their use as a calcium sulfate source, making this practice even more environmentally and economically beneficial [14].

From a chemical point of view, phosphogypsum (PG) - a by-product in the phosphate fertilizer industry - is an excellent potential calcium sulfate source. However, PG can be classified as a naturally occurring radioactive material (NORM) due to elevated concentrations of radium [15,16]. PG also contains impurities such as phosphates, fluorides, heavy metals and other trace elements [16], placing many restrictions on its reuse. The impurity composition is greatly dependent on the origin of the phosphate rock used and to a lesser extent on differences in process plant operation and the PG's age. PG is currently being added to stacks at an annual rate of about 100-280 million tons worldwide [16], and approximately 3 billion tons have already been stacked in well over 50 countries [17]. Furthermore, the production of PG is expected to increase in the coming decades as a consequence of rising food demand. Basic and applied research is necessary to widen its field of application, provided that such practice will not cause additional risks to the public or the environment.

The reuse of NORM in building materials requires radiological characterization because it can enhance both the external and internal dose rate for residents, induced by gamma

radiation and the inhalation of radon, respectively [18–21]. In this respect, indexes are commonly used as a screening aid in the decision whether or not a NORM can be used for building purposes. In other words, (partially) NORM-based building materials may not exceed levels stated in the index used. Current Chinese and Russian legislation is based on the calculation of the radium equivalent index (Ra_{eq}) [22,23]. In European countries, the gamma dose rate imposed by building materials is regulated by the European Basic Safety Standards (EU-BSS), which operate on the calculation of the activity concentration index (ACI) [24]. However, there exist no specific regulations concerning radon release from building materials, although this should be kept as low as possible as this radionuclide is classified by the International Agency for Research on Cancer (IARC) as a Group 1 human carcinogen [25] in the case of long term exposure. Radon can be released from the solid matrix by recoil when radium decays (referred to as emanation) and leaves the building material through the pore network (referred to as exhalation) by diffusion or advective flow [26]. There exist three naturally occurring radon isotopes (i.e., ^{219}Rn, ^{220}Rn and ^{222}Rn), but only ^{222}Rn is generally of significance from the radiation protection point of view [27] and hence is further considered in this study.

Upon reuse, the presence of impurities contained in the PG may not lead to secondary pollution. Ettringite ($(CaO)_6(Al_2O_3)(SO_3)_3.32H_2O$, or in cement chemists' notation $C_6A\bar{S}_3H_{32}$), however, can incorporate a number of ions in its crystal structure [28–30] and therefore act as an immobilization agent. The effectiveness of such immobilization can be evaluated by a leaching assessment. In this respect, a column test provides reliable field-correlated information [31]. On the European level, the CEN/TC 351 [32] provides valuable guidance for testing the release of dangerous substances from construction products into soil, surface water and ground water, including the column leaching protocol CEN/TS 16637-3 [33], which is applied in this study.

In this investigation, ettringite-based mortars from LS and PG are developed for use as an alternative binder for OPC in the building industry. Since PG is considered as NORM, the

radiological impact (i.e., gamma dose rate and the release of radon) is evaluated. The microstructural features are evaluated using scanning electron microscopy (SEM) coupled with X-ray energy dispersive spectroscopy (EDS). The immobilization of impurities is assessed by means of an up-flow percolation leaching test according to the CEN/TS 16637-3. Nitrogen adsorption/desorption was applied to investigate the porosity features. This study complements a parallel study wherein the hydration, mineralogy and compressive strength were investigated for the same binder mixtures [34].

2. Materials and methods

2.1 Materials

The LS was provided by SSAB Europe Oy (Raahe, Finland) after exposure to natural conditions at its cooling pit. The free CaO content was measured following EN 450-1 [35] and found to be zero. The LS was ball-milled (TPR-D-950-V-FU-EH, Germatec Germany) to obtain a d_{50} value of 10 µm. As calcium sulfate source, 3 different products were used (hereafter referred to as G1, G2 and G3, respectively). G1 constituted synthetic $CaSO_4.2H_2O$, supplied by VWR (product code 22451.360). G2 was PG provided by Yara Oy (Finland). G3 was PG collected from a plant in Gdansk (Poland) and was milled and homogenized by the International Atomic Energy Agency (IAEA) (reference material n° 434) [36]. To remove excess moisture, G2 was dried at 333.15 K in a laboratory oven for 24 h. The particle size distribution of LS, G1, G2 and G3 is presented in [34]. No additional milling was performed for G2 and its unimodal particle size distribution ranged from 0.1 µm to 324 µm. G1 and G3 were used as received with unimodal particle size distributions ranging from 0.2 µm to 66 µm and from 0.2 µm to 24 µm, respectively. The d_{50} value for LS, G1, G2 and G3 was 10 µm, 12 µm, 66 µm and 7 µm, respectively. X-ray fluorescence analysis (XRF) (Philips PW 1830) was applied to obtain the chemical composition of the LS and G2. The matrix composition of G3 was provided by the IAEA and was: 96 wt% $CaSO_4.2H_2O$, 1-2 wt%

129 P_2O_5, 1.2 wt% F^-, 1 wt% SiO_2 and 0.2 wt% Al_2O_3 [36]. The chemical composition of the
130 materials is summarized in Table 1.

131 **Table 1**: Chemical composition (in wt%) of LS, G1, G2 and G3

	LS	G1	G2	G3
CaO (C)	51.1	41.2	45.9	39.5
SiO_2 (S)	14.1	-	0.2	1.0
Al_2O_3 (A)	24.6	-	0.3	0.2
Fe_2O_3 (F)	0.5	-	-	-
SrO	32.2 10^{-3}	-	0.8	-
MgO	3.8	-	0.2	-
SO_3^- ($\bar{S}$)	0.4	58.8	51.4	56.5
TiO_2	4.2	-	-	-
CeO_2	-	-	0.3	-
P_2O_5	-	-	0.6	1.5
F^-	-	-	-	1.2
MnO	1.1	-	-	-
Others	0.2	-	0.3	0.1

132

133 A Bruker D2 PHASER was operated at 30 kV and 10 mA to investigate the mineralogy of the
134 LS, G1, G2 and G3, which is summarized in Table 2. A counting time of 0.3 s per step with a
135 step size of 0.02° was used for examinations over the range from 5° to 70° 2θ in continuous
136 PSD fast mode. Prior to the measurement, the powders were mixed with 10 wt% of
137 analytical-grade crystalline ZnO (99.9% purity, Merck) as an internal standard. The samples
138 were prepared using the back loading technique. During the measurement, an anti-scatter
139 slit was positioned 1 mm above the samples and they were rotated at 15 rpm. Qualitative
140 analysis was performed with EVA V.3.1 (Bruker AXS). MAUD (Material Analysis Using

Diffraction) [37] was used for quantitative analysis based on the Rietveld method [38]. The phase contents were recalculated based on the known initial ZnO content.

Table 2: Mineralogy (in wt%) of LS, G1, G2 and G3

	LS	G1	G2	G3
Calcio-olivine ($\gamma-C_2S$)	21.0	-	-	-
Tricalcium-aluminate (C_3A)	2.3	-	-	-
Mayenite ($C_{12}A_7$)	21.9	-	-	-
Periclase (MgO)	2.1	-	-	-
Perovskite ($CaTiO_3$)	1.3	-	-	-
Calcium aluminum magnesium silicate ($Ca_{20}Al_{26}Mg_3Si_3O_{68}$)	47.3	-	-	-
Gypsum ($C\bar{S}.2H$)	-	96.8	93.6	33.2
Bassanite ($C\bar{S}.0.5H$)	-	-	6.4	27.1
Anhydrite ($C\bar{S}$)	-	3.2	-	32.1
Amorphous	4.0	-	-	7.6

2.2 Gamma spectroscopy

About 300 g of homogenized LS and G2 were stored in an airtight polystyrene cylindrical container of 250 cm³ with metal screwcap for 30 days to attain radioactive equilibrium of ^{226}Ra and ^{228}Th and their progenies. G1 is assumed to contain a negligible amount of naturally occurring radionuclides (NOR) and the NOR content of G3 was provided by the IAEA. The measurements were performed using a High-Purity Germanium (HPGe) detector (Mirion Technologies, Canberra, model BE5075-7500SI), coupled with a Lynx multi-channel analyzer. Details of the HPGe detector and technique have been given elsewhere [27]. The ^{234}Th activity concentration was estimated from the 63.3 keV (3.75%) gamma peak. The

^{226}Ra activity concentration (A_{Ra-226}) was estimated from the 609.3 keV (45.5%), 1120.3 keV (14.9%), 1729.6 keV (2.8%) and 1764.5 keV (15.3%) gamma peaks from ^{214}Bi and from the 351.9 keV (35.6%) gamma peak from ^{214}Pb. The ^{210}Pb activity concentration was estimated from its 46.5 keV (4.2%) gamma peak. The ^{232}Th activity concentration (A_{Th-232}) was estimated from the 911.2 (26.2%) gamma peak from ^{228}Ac and from the 238.6 (43.6%) gamma peak from ^{212}Pb. The activity concentration of ^{208}Tl was estimated from the 583.2 keV (85.0%) gamma peak and was corrected for branching [39]. The ^{40}K activity concentration (A_{K-40}) was estimated using the 1460.8 keV (10.6%) gamma peak from ^{40}K itself. The decay data are taken from the DDEP (Decay Data Evaluation Project) [40]. The ^{235}U decay chain is not considered in this study because of its low abundancy.

2.3 Sample synthesis

By varying the ratios of LS, G1, G2 and G3 in the binder, a total of 7 mortar samples (M0-M6) were prepared. The binder mixtures are shown in Table 3. As set retarder, a 0.5 wt% citric acid solution was prepared by dissolving citric acid (supplied by Tokyo Chemical Industry Co., Ltd., Japan, product code C1949) in distilled water (ASTM type II) using magnetic stirring at a speed of 250 rpm for 30 min at room temperature. The mortar samples were prepared according to EN 196-6 [41] using CEN standard sand (DIN EN 196-1) with a sand-to-binder ratio (S/B) of 3. The liquid-to-binder ratio (L/B) was established at 0.45 based on previous experimental work [9]. After mixing, the mortars were cast in silicon cubic molds of 3.5 cm × 3.5 cm × 3.5 cm, whereafter the molds were stored in sealed plastic bags to avoid the evaporation of water. The samples were demolded after 24 h and further cured for 28 days in a water bath at room temperature. After 28 days of curing, samples were air-dried at room temperature for 2 days, whereafter they were dried in a laboratory oven at 313.15 K for 2-3 days until a constant weight was achieved. Prior to testing, the mortar samples were cooled down to room temperature in a desiccator. For SEM/EDS, paste samples were prepared with a L/B of 0.45. After mixing, the casting and curing regimes were similar as for

the mortars. After their curing period, the hydration of the pastes was stopped by solvent exchange using isopropanol.

Table 3: Binder mixtures (in wt%)

	LS	G1	G2	G3
M0	70	30	0	0
M1	70	20	10	0
M2	70	10	20	0
M3	70	0	30	0
M4	70	20	0	10
M5	70	10	0	20
M6	70	0	0	30

2.4 Calculation of indexes for screening of gamma dose rate

Based on the binder mixtures presented in Table 3, the Ra_{eq} [22,23] and the ACI [24] were calculated (Eq. 1 and Eq. 2, respectively) for both paste and mortar samples allowing a conservative screening. For mortar samples, the mass of the standard sand was included and it was assumed that there are no NOR present in the standard sand.

$$Ra_{eq} = A_{Ra-226} + 1.43\, A_{Th-232} + 0.077\, A_{K-40} \quad (Eq.\,1)$$

$$ACI = \frac{A_{Ra-226}}{300\ Bq/kg} + \frac{A_{Th-232}}{200\ Bq/kg} + \frac{A_{K-40}}{3000\ Bq/kg} \quad (Eq.\,2)$$

A Ra_{eq} value lower than 370 Bq/kg suggests an indoor external gamma exposure below 1.5 mSv/y [42], while an ACI below 1 indicates a possible indoor external gamma exposure below 1 mSv/y [24]. In case the Ra_{eq} value of a given material exceeds the reference level of 370 Bq/kg, the potential applications of such a material are categorized as follows: (1) Ra_{eq}< 370 Bq/kg: for building residential houses; (2) 370 Bq/kg < Ra_{eq} < 740 Bq/kg: for industrial

use; (3) 740 Bq/kg < Ra_{eq} < 2200 Bq/kg: for roads and railways; (4) 2200 Bq/kg < Ra_{eq} < 3700 Bq/kg: for landfilling; and (5) Ra_{eq} > 3700 Bq/kg: forbidden to use for any construction [43]. The ACI is applied for building materials (e.g. concrete, ceramics, bricks or gypsum board) or their constituents if they are also building materials. In case those constituents are separately assessed, an appropriate partitioning factor needs to be applied. If the ACI exceeds the value of 1, an elaborated dose calculation needs to be executed to evaluate whether their use in building applications is justified [44,45].

2.5 Radon exhalation and emanation

The radon exhalation (Ex_{Rn}) (in Bq/(kg*h)) of the mortars was determined with a SARAD RadonScout PMT radon monitor (Lucas cell, ZnS scintillator with an active volume of 0.3 dm³) by enclosing the sample in a plexiglass accumulation chamber of 2 dm³. The measurement of the radon concentration (C) (in Bq/m³) was performed as previously described in [27]. The accumulation period ranged from 3-4 days and the measurements were executed in triplicate under laboratory conditions (temperature 293.15 ± 2 K, relative humidity about 50%). Since only ^{222}Rn is considered, C was calculated from the data obtained in the interval from 2.5-4.0 h after the pump was stopped. The Ex_{Rn} was calculated by the slope of the initial linear region of C, according to Eq. 3 [46]:

$$Ex_{Rn} = \left[\frac{C\ V}{m\ t}\right]\left[\frac{\lambda^*\ t}{1 - \ e^{-\lambda^*\ t}}\right] \quad (Eq.3)$$

where V is the volume of the accumulation chamber (in m³), m is the mass of the mortar sample (in kg), t is the time (in h) and λ^* (/h) is the effective ^{222}Rn decay constant (determined as explained in [27]). The emanation factor Em_{Rn} (in %) is calculated using the A_{Ra-226} of the mortar samples from the 30th day with Eq. 4 [47]:

$$Em_{Rn} = \frac{A_{Rn}^{out}}{A_{Ra}^{in}}\ 100 \quad (Eq.4)$$

where A_{Rn}^{out} is the calculated radon activity in the chamber after accumulation (in Bq) and A_{Ra}^{in} is A_{Ra-226} (in Bq).

2.6 Microstructural analysis

The microstructure of paste samples was evaluated through SEM using a Zeiss Ultra Plus instrument with a 15 kV accelerator voltage and a working distance of 7-8.5 mm. Prior to evaluation, the pastes were vacuum-impregnated with epoxy resin, whereafter they were polished using diamond discs of 220-1 µm at 150 rpm with ethanol as lubricant. The pastes were observed using backscattered electrons (BSE). EDS was used to determine the chemical compositions.

2.7 Leaching assessment

The leaching of mortar samples was assessed with an up-flow percolation test on granular material, according to CEN/TS 16637-3 [33]. The sample preparation, measurement circumstances, experimental set-up and the execution of the leaching test were the same as in [48]. Distilled water (ASTM type II) was chosen as leachant solution. After a saturation period of 20 h, 7 eluate fractions were collected at predefined intervals (0.10 ± 0.02 l/kg, 0.10 ± 0.02 l/kg, 0.30 ± 0.05 l/kg, 0.50 ± 0.05 l/kg, 1.00 ± 0.05 l/kg, 3.0 ± 0.1 l/kg, 5.0 ± 0.2 l/kg) until a cumulative liquid-over-solid ratio (L/S) of 10.0 ± 0.5 l/kg was obtained. Immediately after collection, the pH (HI2211 pH/ORP Meter, HANNA Instruments) and conductivity (Konduktometer CG 858, Schott Geräte) of each eluate fraction were measured. During the leaching test, the bottles for collection of the eluates were covered with plastic foil in order to minimize carbonation. The eluate fractions were analyzed by inductively coupled plasma optical emission spectrometry (ICP-OES, Perkin Elmer Optima 8300, RSD < 2%) for analysis of Al, Ca, Ce, Fe, Mg, Mn, P, S, Si, Sr and Ti and ion-chromatography (IC, Dionex DX120) for analysis of F. For IC, an analytical column (IonPac AS14A) equipped with a conductivity

detector was used, the pH of the eluates was buffered using 1 mM $NaHCO_3$ (supplied by Merck) and 8 mM Na_2CO_3 (supplied by Merck).

2.8 Nitrogen adsorption/desorption

Nitrogen adsorption/desorption tests were carried out by a TRISTAR 3000 Micromeritics device at 76.95 K. Prior to measurements, mortar samples were degassed using the flowing degas process at 312.95 K under nitrogen flow for 12 h, with an input relative pressure of 2×10^5 Pa. The specific surface area was derived from the nitrogen adsorption data over the P/P_0 range of 0.05-0.30 (where P is the partial vapor pressure of the adsorbate gas in equilibrium and P_0 is the saturated pressure of the adsorbate gas at 76.95 K) by the BET (Brunauer, Emmett and Teller) method [49]. The Barrett-Joyner-Halenda (BJH) interpretation was used to evaluate the mesopore size distribution and cumulative mesopore volume from the adsorption isotherm [50]. The T-plot analysis method [51] was applied for determination of the micropore volume and micropore specific surface area from the adsorption data.

3. Results and discussion

3.1 Gamma spectroscopy

The activity concentrations of the NOR are summarized in Fig. 1. The NOR content of G1 is assumed to be negligible. Secular equilibrium between radium and progeny was established for both the ^{238}U (^{226}Ra) and ^{232}Th (^{228}Ra) decay chains, as the activity concentration ratios $^{214}Pb/^{214}Bi$ and $^{228}Ac/^{212}Pb$ ranged from 1.01 to 1.04 and 0.96 to 0.98, respectively [39]. World average concentrations of ^{226}Ra, ^{232}Th and ^{40}K in the earth's crust are 40 Bq/kg, 40 Bq/kg and 400 Bq/kg, respectively [52]. When comparing those values with the ones presented in Fig.1, it is concluded that only G3 contains enhanced levels of NOR (more particularly ^{226}Ra and progeny) as a consequence of its industrial processing [53]. G2 is characterized by a very low natural radioactivity compared to the overall average in 12 EU member states

corresponding to 381 Bq/kg ^{226}Ra, 22 Bq/kg ^{232}Th and 71 Bq/kg ^{40}K in PG [21], which is promising from the valorization point of view. For the LS, the NOR from the ^{238}U decay chain were the most abundant compared to those from the ^{232}Th decay chain, while the opposite is observed for G2. This is a consequence of the terrestrial radionuclides from natural origin present in the mineral ore that has been processed. The presence and concentration of ^{232}Th in G2 are uncertain as ^{232}Th cannot be measured directly by gamma spectroscopy, though its concentration was equated with the ^{228}Ra activity concentration in this study. However, one should keep in mind that the latter is only valid if there is secular equilibrium in the upper part of the ^{232}Th decay chain. The measured intensities of ^{40}K and ^{234}Th were below the detection limit for G2. This was also the case for ^{40}K, ^{228}Ac, ^{212}Pb and ^{208}Tl for G3. Pb becomes volatile in high-temperature environments, which explains the reduced activity concentration of ^{210}Pb for LS that is generated by high-temperature processing.

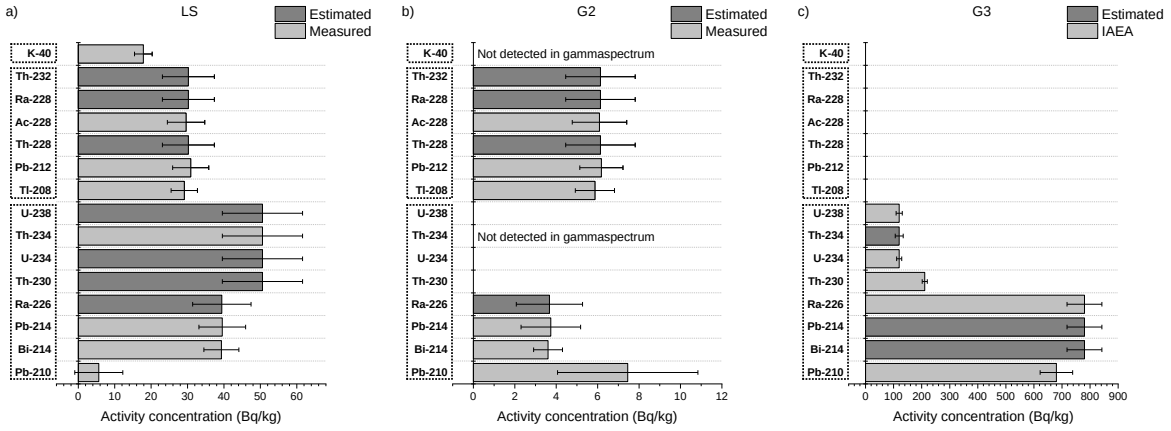

Figure 1: Activity concentrations (in Bq/kg, 2σ error) for a) LS, b) G2 and c) G3

The Ra_{eq} and the ACI were calculated with Eq. 1 and Eq. 2, respectively, for both paste and mortar samples, and the results are presented in Fig. 2. It can be observed that the ACI is stricter compared to the Ra_{eq}. For all samples, the calculated mean Ra_{eq} and ACI were below the reference levels of 370 Bq/kg and 1, respectively, meaning that both paste and mortar samples can directly be used as building material without radiological constraints. Taking into account the 2σ error, the ACI for M6 (as a paste) was 0.98 ± 0.11 and

consequently exceeded slightly the reference level of 1. It has to be emphasized once more that these indexes only serve as a conservative screening tool. Because pastes and mortars are not directly used as a structural part of a building, it is more straightforward (and legally relevant) to evaluate the ACI of concrete. Besides, aggregates used in concrete production can also possess NOR. This could either increase or dilute the total NOR content, which has to be evaluated for each specific case. Also the possible heterogeneity of industrial by-products needs to be taken into account. The databases on NORM in construction materials developed as part of the European COST Action TU1301 'NORM4BUILDING' [54] are a valuable aid here.

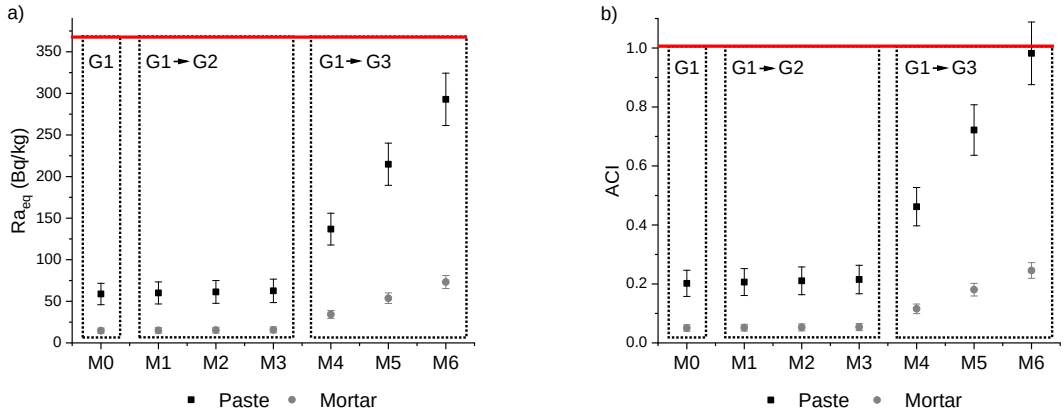

Figure 2: a) Ra_{eq} and b) ACI calculated for paste and mortar samples

3.2 Radon exhalation and emanation

The Ex_{Rn} and Em_{Rn} of mortar samples after 28 days of curing, calculated with Eq. 3 and Eq. 4, respectively, are shown in Fig. 3. The ^{226}Ra activity concentration of G2 was already very low (3.7 ± 1.6 Bq/kg) and consequently the substitution of G1 by G2 does not amend the overall ^{226}Ra activity concentration. Therefore, the Ex_{Rn} and Em_{Rn} of samples M0, M1, M2 and M3 are in the same order of magnitude (roughly around 30 mBq/(kg*h) and 50%, respectively). Compared to literature on mortars from standard cement (0.1 to 2.3 mBq/(kg*h) and 5 to 42% [47,55–58]) and mortars from (alkali-activated) NORM streams (6

to 12 mBq/(kg*h) [27,59] and 2 to 3.7% [55,59]) characterized by ^{226}Ra activity concentrations of the same range and approximately the same density, these values are slightly higher. Upon substituting G1 by G3, the ^{226}Ra activity concentration of samples M4, M5 and M6 gradually increases. Consequently the Ex_{Rn} becomes slightly higher, i.e., 88.5 ± 4.5 mBq/(kg*h), 78.8 ± 3.5 mBq/(kg*h) and 98.3 ± 2.8 mBq/(kg*h) for M4, M5 and M6, respectively. By contrast, the Em_{Rn} was the lowest among all samples, with values ranging from 36.8 ± 3.8% to 16.5 ± 0.9%. The Em_{Rn} is of particular interest because it indicates how large the fraction of the total ^{222}Rn generated is free to leave the building material, for which M6 was the best performing sample in this study. Assuming that the ^{226}Ra atoms are homogeneously distributed throughout the samples and supposing an equal density, Em_{Rn} is determined particularly by the microporosity [46,60,61]. This is consistent with Fig. 9 (see further in section 3.5), where it is observed that both the volume and specific surface area of the micropores decreases when moving from M4 to M6. At the same time, the mesoporosity increases from M4 to M6 and consequently does not appear decisive regarding Em_{Rn}.

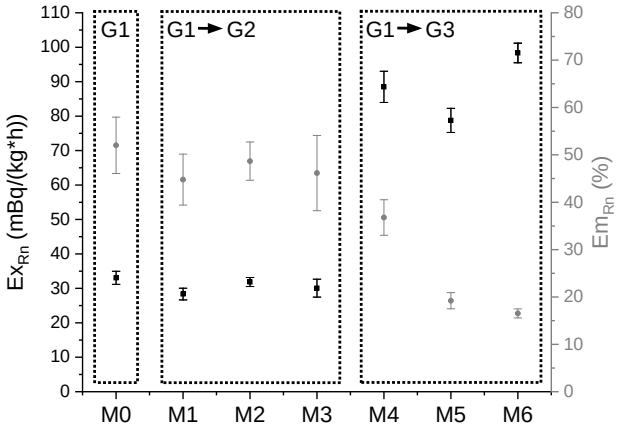

Figure 3: Ex_{Rn} and Em_{Rn} of mortar samples after 28 days of curing

3.3 Microstructural analysis

The microstructural analysis revealed the presence of ettringite (AFt), monosulfate (AFm),

aluminium-hydroxide (AH_3), and an amorphous calcium-(alumino)-silicate-hydrate gel (C-(A)-S-H) as hydration products, which are indicated in Fig. 4a and Fig. 4b.

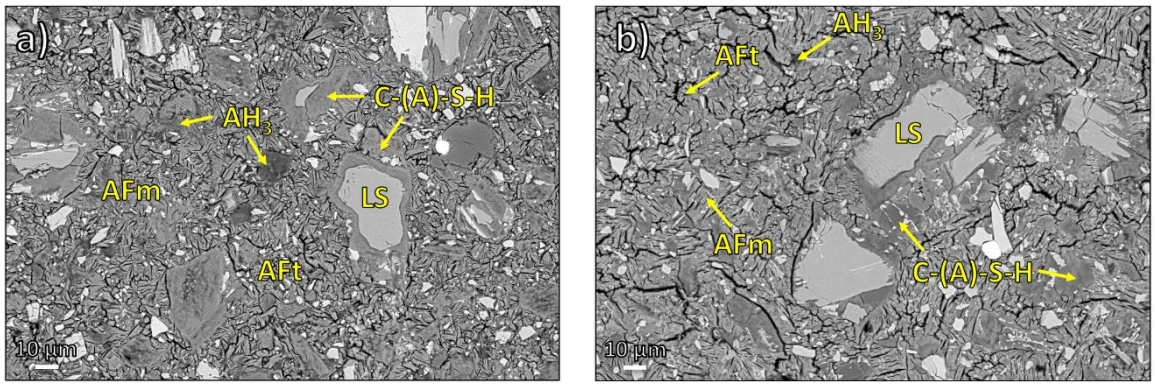

Figure 4: BSE image of a) M0 (paste, LS and G1) and b) M6 (paste, LS and G3)

The atomic ratios Al/Ca versus Si/Ca and Ca/Al versus S/Al, obtained from EDS (spots were randomly distributed), are presented in Fig. 5. From Fig. 5a, it can be seen that there was a relatively high level of intimate mixing of C-(A)-S-H with other hydration products [62], evidenced by the cloud of data points. The C-(A)-S-H phase is characterized by a low Si/Ca atomic ratio, which is in line with the low reactivity of $\gamma-C_2S$ [63,64]. It is worth mentioning that, based on thermodynamic modelling of the pastes, strätlingite is thermodynamically favorable in the system [65,66]. Hence, the C-(A)-S-H phase may convert to strätlingite after extended curing periods. Fig. 5b plots the chemical composition of ettringite (AFt), monosulfate (AFm, likely including its solid solutions), and aluminium-hydroxide (AH_3). Monocarbonate was found in neither of the pastes. When gypsum gets substituted by PG (i.e., the substitution of G1 by G3) (the green dots), the data move towards the binary composition of aluminium-hydroxide (AH_3) and ettringite (AFt). By contrast, the use of G1 (the black dots) gave rise to the formation of monosulfate (AFm). Additional information about the phase assemblage and their characterization is presented in [34]. The role of those hydration products in leaching performance is elucidated in section 3.4.

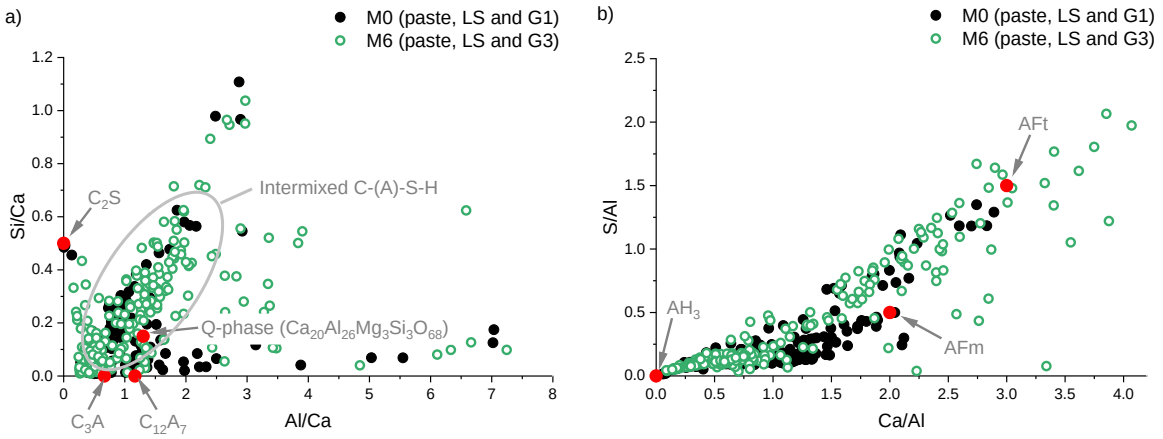

Figure 5: Atomic ratios obtained from EDS for a) Al/Ca versus Si/Ca and b) Ca/Al versus S/Al (red dots represent the theoretical atomic ratios of the phases indicated)

3.4 Leaching assessment

The leaching of inorganic elements from the granulated mortars was assessed by an up-flow percolation column test according to CEN/TS 16637-3 [33]. Fig. 6 shows the pH of the eluate fractions, which was measured immediately after collection. The substitution of G1 by G2 did not influence the eluate pH (Fig. 6a), while substitution by G3 resulted in a slightly lower eluate pH (Fig. 6b). The stability domain for ettringite lies generally in the range from 10.5 to 13.0 [67], while the calcium-silicate-hydrate phase (C-S-H) starts to dissolve at a pH of around 11 [68].

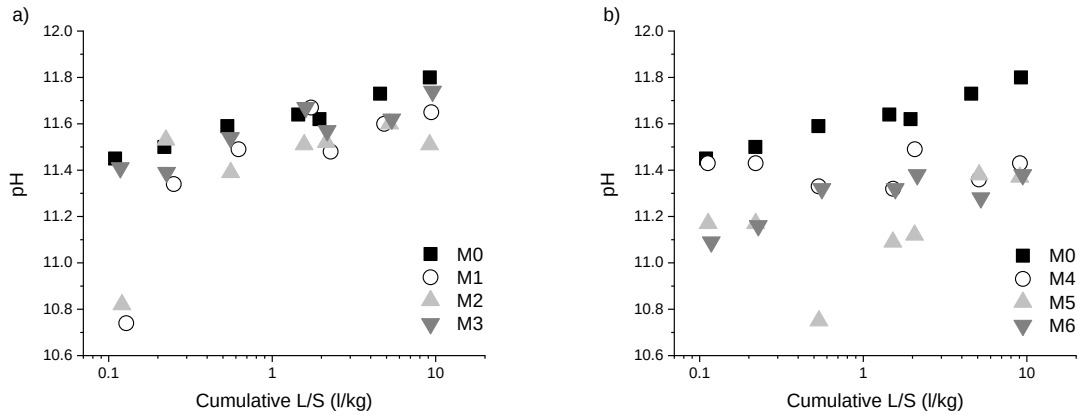

Figure 6: Eluate pH as a function of cumulative L/S upon substituting G1 by a) G2 and b) G3

Fig. 7 shows the concentrations of Al, Ca, F, Fe, Mg, S, Si and Sr in the eluates. The concentrations of Ce, Mn, P and Ti were below the detection limit (0.01 mg/l, 0.01 mg/l, 0.10 mg/l and 0.05 mg/l, respectively) in each case. For Al and Ca, the quantities present in the eluates ranged from 25 to 150 mg/l and from 70 to 160 mg/l, respectively. For the other elements (i.e., F, Fe, Mg, S, Si and Sr), the concentrations were generally much lower, not exceeding 22 mg/l. F was only present in G3 and therefore only measured for M4, M5 and M6. For each element, except for Fe, the concentrations were variable during the experiment and generally decreased when the L/S was increased. An increasing S concentration in the eluates would indicate the decomposition of ettringite, which is not the case in this study. From these patterns, the release mechanism for each individual element can be determined, as described in CEN/TS 16637-3 [33]. The latter is useful in order to predict the long term release during in-use and end-of-life situations of the material. The following release mechanisms were identified: apparent depletion for Al and Sr; solubility controlled release for Ca; and depletion for Mg. The overall release mechanisms for F, Fe, S and Si were variable and remained unidentified.

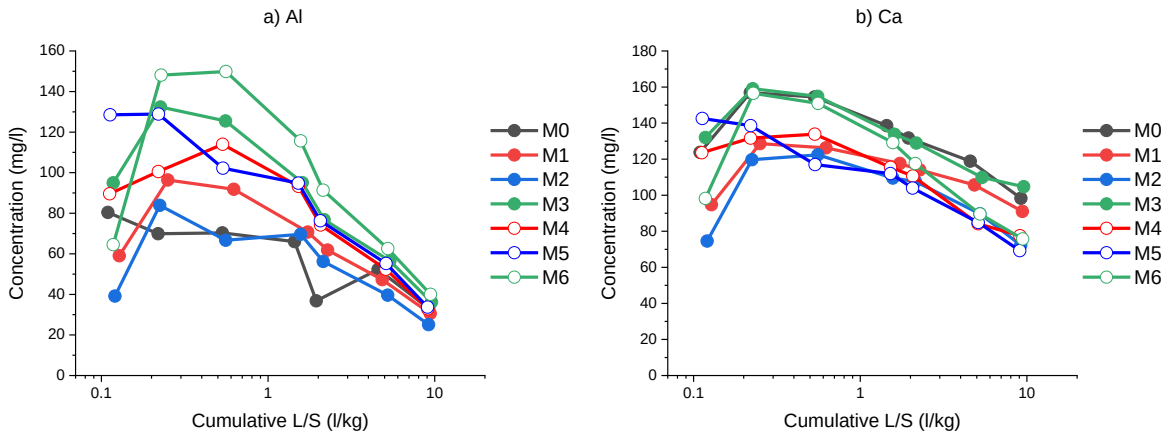

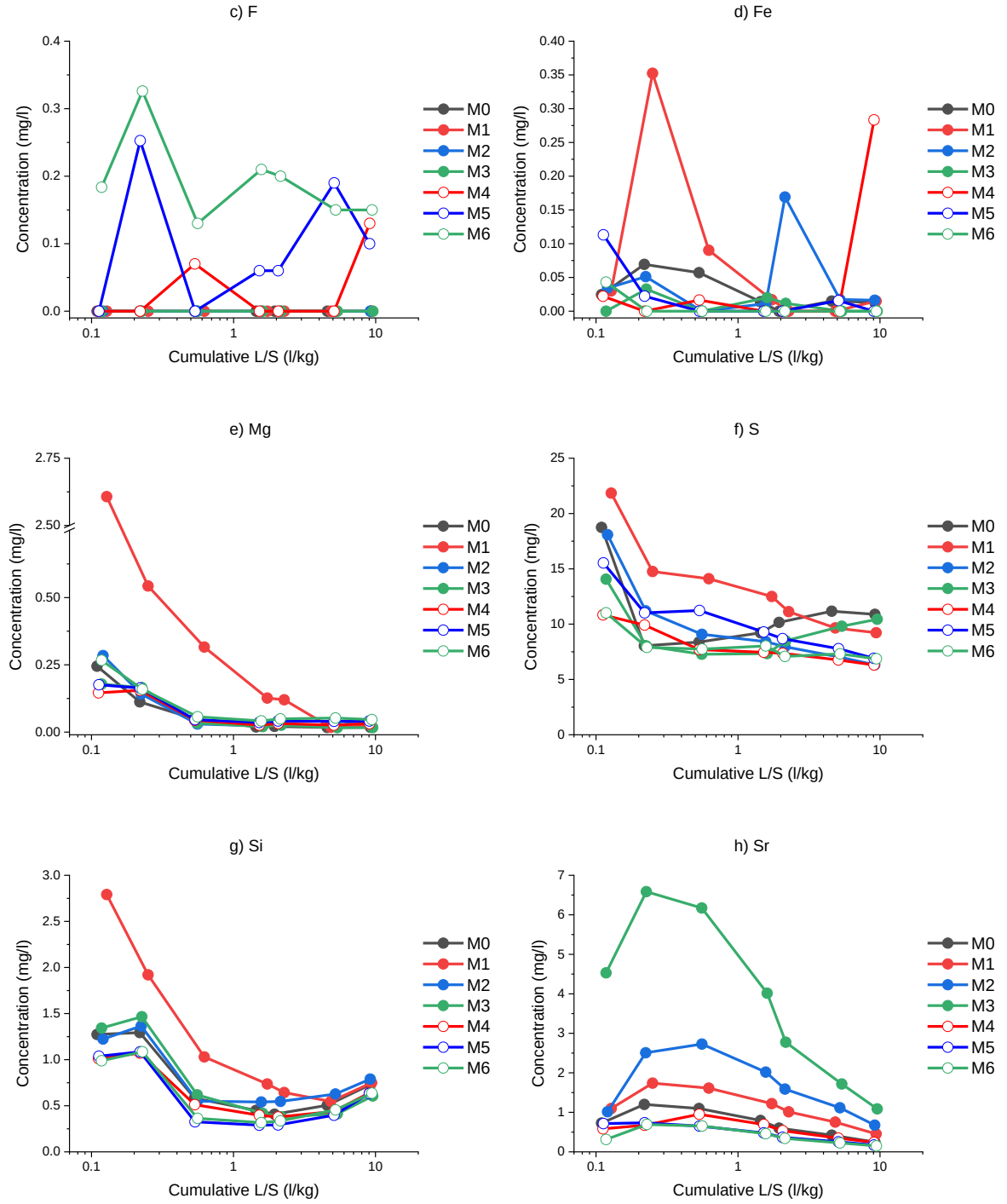

Figure 7: Concentrations as a function of cumulative L/S for a) Al, b) Ca, c) F, d) Fe, e) Mg, f) S, g) Si and h) Sr

From the cumulative release (in mg/kg) at an L/S of 10.0 ± 0.5 l/kg (calculated from the data in Fig. 7) and the elemental concentration of the samples (in mg/kg) (calculated from the data in Table 1), the relative release was calculated and is shown in Fig. 8.

Immobilization of contaminants occurs by either physical or chemical processes or by a combination thereof, as well as by the transport of dissolved ions to the eluate solution [69]. In case of retention by chemical means, the contaminant becomes part of the hydration products by cation or oxyanion substitution. The ettringite structure can incorporate a number of different ions, which is enviable for immobilization [30,70–72]. Trivalent ions can substitute Al^{3+} in the ettringite structure [71], while bivalent ions can replace Ca^{2+} [29]. An example is Fe-substituted ettringite ($C_6(A,F)\bar{S}_3H_{32}$) [68]. At the same time, SO_3^- can be replaced by metal oxyanions [72]. However, it is most likely that the dominant anion (SO_3^-) forms ettringite, while the remaining oxyanions either form monosulfate or interact by another mechanism (i.e., sorption or physical inclusion) [72]. It has to be noted here that detailed X-ray diffraction data on the existence of ettringite and monosulfate phases are presented in a parallel study on the same binder mixtures [34]. However, ettringite does not seem to be more effective in the immobilization of oxyanions than monosulfate [72]. Since the leaching behavior of S is comparable for all samples (see Fig. 7f), the competition degree between SO_3^- and other oxyanions for exchange sites in the ettringite (or monosulfate) structure is comparable and independent of the (phospho-)gypsum source used. Next to ettringite, aluminium-hydroxide and an amorphous C-(A)-S-H are found to constitute an important part of the hydration products (see section 3.3). Aluminium-hydroxide is not significant regarding immobilization [72]. On the other hand, immobilization by the C-(A)-S-H structure is more efficient for cations because (1) Ca^{2+} can be substituted by bivalent cations and (2) the sorption capacity for anions decreases with increasing pH [73]. This emphasizes that ettringite plays an important role in oxyanion immobilization. The formation of insoluble (hydr-)oxides and their physical encapsulation cannot be excluded.

The degree of stabilization for Ce, Mn, P and Ti is equal or nearly equal to 100% for all samples, as their concentrations in the eluates were below the detection limit. At alkaline pH, Ce is expected to precipitate as insoluble CeO_2 or $Ce(OH)_3$. However, Ce^{3+} could also be incorporated into the ettringite and/or C-(A)-S-H structure. The same scenario is expected for

Mn, which can precipitate as Mn_3O_4 or $Mn(OH)_2$, or get incorporated as Mn^{2+} or Mn^{3+} in the ettringite and/or C-(A)-S-H phase. P is likely incorporated in the ettringite structure as HPO_4^{2-}. Ti transforms to anatase (TiO_2) in alkaline media or could be incorporated as Ti^{2+} or Ti^{3+} in the hydration products. The relative release of F was comparable for mortars incorporated with Polish PG (M4, M5 and M6) and ranged from 0.19 to 0.20%. In alkaline cementitious matrices, F precipitates as insoluble CaF_2 [74,75]. However, F could also get incorporated in the ettringite structure at the SO_4^{2-} site, or in other mineral phases (such as fluorellestadite) [76,77]. The immobilization of Fe occurred most likely by the formation of Fe-substituted ettringite. Fe release was highest for M4 (0.2%) and lowest for M6 (9.2×10^{-4} %), while M0 showed a release of 0.2×10^{-1} %. Mg release was very low and ranged from 0.5×10^{-2} to 0.2×10^{-1} %. Consequently, the immobilization degree exceeded 99.9% for all samples. Since both Mg and Sr belong to the group of alkaline earth metals, they behave similarly to Ca and can be incorporated in both the ettringite and C-(A)-S-H phase as Mg^{2+} and Sr^{2+}. Mortars incorporated with Finnish PG (M1, M2 and M3) exhibit better fixation of Sr than those from G1 (M0) and Polish PG (M4, M5 and M6). However, the degree of stabilization is over 90% in each case. Sr release increases upon substitution of G1 by G2, while the reverse is seen upon substitution of G1 by G3. The relative release for M0 was highest and amounted to 8.4%. For the more prominent elements (Al, Ca, S and Si) the relative release was comparable for all samples (1.8 - 2.9%, 1 - 1.4%, 0.5 - 0.7% and 0.04 - 0.06%, respectively), indicating that the same hydration products at comparable levels and stability were formed in all samples, irrespective of the (phospho-)gypsum source used. According to the European Drinking Water Directive [78], the Al and Fe concentration of (part of) the eluates exceeded the parametric value (0.2 mg/l and 0.2 mg/l, respectively). Nevertheless, the pH for drinking water purposes should be equal to or lower than 9.5 [78].

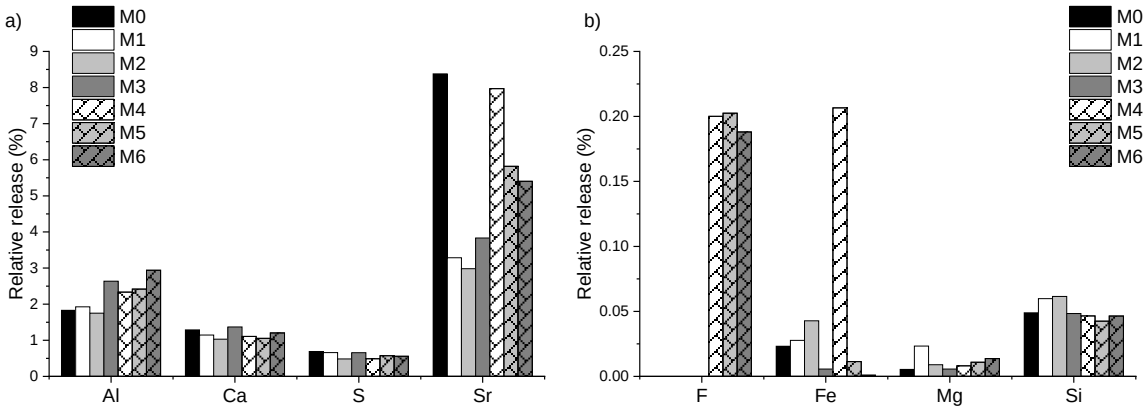

Figure 8: Relative release of a) Al, Ca, S, Sr and b) F, Fe, Mg, Si

The stability of the ettringite structure (both pH and temperature dependent) plays an important role in unceasing immobilization. The conversion of ettringite to monosulfate is not expected to be disastrous, as the monosulfate phase shows comparable or even better immobilization potential [72]. However, when monosulfate converts again to ettringite at later ages (delayed ettringite formation, DEF), catastrophic expansion occurs, potentially leading to high release rates, failed immobilization and even environmental pollution. Because, in real-life, multiple factors are simultaneously acting on building/construction materials (such as (acid) rainfall, frost, growth of bacteria and fungi, carbonation, contact with seawater or agricultural polluted waters, sulfate bearing groundwater, among others), possessing synergistic and/or catalytic effects, extrapolation of lab-scale leaching tests to in-use and end-of-life situations should be done with caution. For this reason, geochemical modeling and an Eh-pH dependent leaching test could be interesting follow-up studies. The latter would also provide confirmation on the preferential immobilization mechanism for each element, since first the C-S-H phase will dissolve at a pH around 11, while ettringite remains stable until a pH of around 10.5. However, one should keep in mind that the pH boundaries of contaminant-substituted-ettringite (such as Fe-substituted-ettringite) can vary [72] and should be carefully sought in order to avoid the generation of misleading results.

3.5 Nitrogen adsorption/desorption

The specific surface area and volume of the micro- and mesopores were assessed by means of nitrogen adsorption/desorption and presented in Fig. 9. Upon the substitution of G1 by G2, the specific surface area of the micropores increased, while the specific surface area of the mesopores decreased. An opposite trend was observed when substituting G1 by G3, where the specific surface area of the micropores decreased and the specific surface area of mesopores increased. The same evolution is seen for the pore volume, with the lowest micro- and mesopore volume obtained for M3. As already mentioned, the microporosity plays a decisive role for radon release. Regarding leaching, it is not straightforward to compare the results from Fig. 9 with leaching data, as the macroporosity should also be included. Despite this, a low porosity is desirable in order to decrease the effects of carbonation among other external factors, which could be detrimental for the stability of the hydration products responsible for contaminant immobilization. Conventional cement shows generally specific surface areas (obtained with nitrogen adsorption/desorption) in the range of 50 m²/g [79], which is 20-30 times higher than the current mortars.

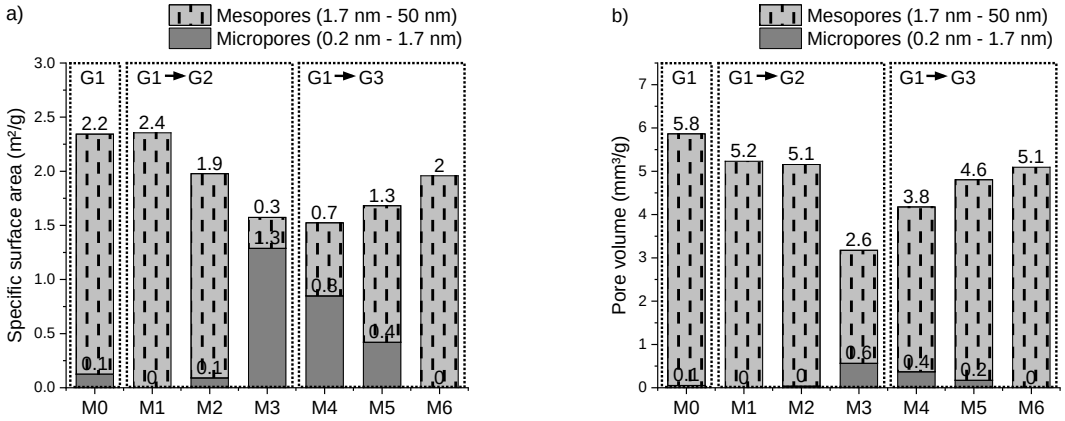

Figure 9: a) Specific surface area and b) pore volume

4. Conclusions

In this study, ettringite-based mortars were produced from LS and PG. Mortars were

480 incorporated with PGs of different origin in variable ratios and were compared with a
481 reference mortar from LS and synthetic gypsum. The used materials showed a variable
482 radionuclide content, which is a consequence of the terrestrial radionuclides from natural
483 origin present in the mineral ore that has been processed. Disequilibrium in the decay chains
484 results from their particular industrial processing. The Ra_{eq} and the ACI were calculated for
485 both paste and mortar samples allowing a conservative screening of the gamma dose rate.
486 In each case, the obtained mean values were below the legal reference levels, indicating that
487 the produced mortars can safely be used for building purposes. The radon emanation
488 decreased upon increasing the Polish PG content. For those mortars, the emanation was
489 mainly determined by the microporosity, while the mesoporosity appeared to be not decisive.
490 The mortars were found to exhibit extremely low micro- and mesoporosity, with specific
491 surface areas between 20-30 times lower than conventional cement (1.5-2.5 m²/g). The
492 immobilization degree for contaminants such as Ce, Mn, P and Ti from PG was equal or
493 nearly equal to 100% for all samples, while retention of F, Fe and Mg exceeded 99% and
494 stabilization of Sr was over 90%. However, extrapolation of lab-scale leaching tests to in-use
495 and end-of-life situations should be done with caution. This investigation shows high potential
496 for PG reuse in ettringite-based mortars.

497

498 **Declarations of interest:** none

499

500 **Acknowledgements**

501 This work was supported by the Fund for Scientific Research Flanders (FWO). The authors
502 would like to thank Jenny Put for the IC measurements and to acknowledge the networking
503 support of the COST Action TU1301, www.norm4building.org. At the University of Oulu, this
504 work was done as part of the FLOW project (project number 8904/31/2017) funded by
505 Business Finland in the ERA-MIN 2 Innovation program (EU Horizon 2020 program). SSAB

Europe Oy and Yara Oy are acknowledged for providing ladle slag and phosphogypsum.

References

[1] C. Shi, A.F. Jiménez, A. Palomo, New cements for the 21st century: The pursuit of an alternative to Portland cement, Cem. Concr. Res. 41 (2011) 750–763. doi:10.1016/j.cemconres.2011.03.016.

[2] H. Motz, J. Geiseler, Products of steel slags an opportunity to save natural resources, Waste Manag. 21 (2001) 285–293. doi:10.1016/S0956-053X(00)00102-1.

[3] D.W. Lewis, Properties and uses of iron and steel slags, National Slag Association, 1982. http://www.nationalslag.org/sites/nationalslag/files/documents/nsa_182-6_properties_and_uses_slag.pdf.

[4] J.M. Manso, M. Losanez, J.A. Polanco, J.J. Gonzalez, Ladle furnace slag in construction, J. Mater. Civ. Eng. 17 (2005) 513–518. doi:10.1061/(ASCE)0899-1561(2005)17:5(513).

[5] V.Z. Serjun, B. Mirtič, A. Mladenovič, Evaluation of ladle slag as a potential material for building and civil engineering, Mater. Tehnol. 47 (2013) 543–550.

[6] E. Adesanya, K. Ohenoja, P. Kinnunen, M. Illikainen, Alkali activation of ladle slag from steel-making process, J. Sustain. Metall. 3 (2017) 300–310. doi:10.1007/s40831-016-0089-x.

[7] E. Adesanya, K. Ohenoja, P. Kinnunen, M. Illikainen, Properties and durability of alkali-activated ladle slag, Mater. Struct. Constr. 50 (2017) 1–10. doi:10.1617/s11527-017-1125-4.

[8] H. Nguyen, V. Carvelli, E. Adesanya, P. Kinnunen, M. Illikainen, High performance cementitious composite from alkali-activated ladle slag reinforced with polypropylene fibers, Cem. Concr. Compos. 90 (2018) 150–160. doi:10.1016/j.cemconcomp.2018.03.024.

[9] H. Nguyen, P. Kinnunen, V. Carvelli, M. Mastali, M. Illikainen, Strain hardening polypropylene fiber reinforced composite from hydrated ladle slag and gypsum, Compos. Part B Eng. 158 (2019) 328–338. doi:10.1016/j.compositesb.2018.09.056.

[10] S. Rubert, C.A. Luz, M.V.F. Varela, J.I.P. Filho, R.D. Hooton, Hydration mechanisms of supersulfated cement: The role of alkali activator and calcium sulfate content, J. Therm. Anal. Calorim. 134 (2018) 971–980. doi:10.1007/s10973-018-7243-6.

[11] A. Gruskovnjak, B. Lothenbach, F. Winnefeld, R. Figi, S.C. Ko, M. Adler, U. Mäder, Hydration mechanisms of super sulphated slag cement, Cem. Concr. Res. 38 (2008) 983–992. doi:10.1016/j.cemconres.2008.03.004.

[12] E.G. Moffatt, M.D.A. Thomas, Durability of rapid-strength concrete produced with ettringite-based binders, ACI Mater. J. 115 (2018). doi:10.14359/51701006.

[13] B.C. McLellan, R.P. Williams, J. Lay, A. Van Riessen, G.D. Corder, Costs and carbon emissions for geopolymer pastes in comparison to ordinary portland cement, J. Clean. Prod. 19 (2011) 1080–1090. doi:10.1016/j.jclepro.2011.02.010.

[14] S. Suarez, X. Roca, S. Gasso, Product-specific life cycle assessment of recycled gypsum as a replacement for natural gypsum in ordinary Portland cement: Application to the Spanish context, J. Clean. Prod. 117 (2016) 150–159.

549 doi:10.1016/j.jclepro.2016.01.044.

550 [15] International Atomic Energy Agency (IAEA), Management of NORM Residues, IAEA-
551 TECDOC-1712, Vienna, 2013.

552 [16] H. Tayibi, M. Choura, F.A. López, F.J. Alguacil, A. López-Delgado, Environmental
553 impact and management of phosphogypsum, J. Environ. Manage. 90 (2009) 2377–
554 2386. doi:10.1016/j.jenvman.2009.03.007.

555 [17] International Atomic Energy Agency (IAEA), Radiation Protection and Management of
556 NORM Residues in the Phosphate Industry, Safety Reports Series No. 78, IAEA,
557 Vienna, 2013. doi:10.1016/j.resourpol.2012.04.002.

558 [18] United Nations Scientific Committee on the Effects of Atomic Radiation (UNSCEAR),
559 Sources and Effects of Ionizing Radiation: UNSCEAR 2008 Report to the General
560 Assembly with Scientific Annexes, New York, 2010.

561 [19] World Health Organization (WHO), Who Handbook on Indoor Radon - A Public Health
562 Perspective, first ed., WHO, Geneva, 2009. doi:10.1080/00207230903556771.

563 [20] K. Kovler, Radiological constraints of using building materials and industrial by-
564 products in construction, Constr. Build. Mater. 23 (2009) 246–253.
565 doi:10.1016/j.conbuildmat.2007.12.010.

566 [21] C. Nuccetelli, Y. Pontikes, F. Leonardi, R. Trevisi, New perspectives and issues
567 arising from the introduction of (NORM) residues in building materials: A critical
568 assessment on the radiological behaviour, Constr. Build. Mater. 82 (2015) 323–331.
569 doi:10.1016/j.conbuildmat.2015.01.069.

570 [22] J. Beretka, P.J. Matthew, Natural radioactivity of Australian building materials,
571 industrial wastes and by products, Health Phys. 48 (1985) 87–95.
572 doi:10.1097/00004032-198501000-00007.

573 [23] C. Nuccetelli, G. de With, R. Trevisi, N. Vanhoudt, S. Pepin, H. Friedmann, G. Xhixha,
574 W. Schroeyers, J. Aguiar, J. Hondros, B. Michalik, K. Kovler, A. Janssens, R. Wiegers,
575 Legislative aspects, in: Nat. Occur. Radioact. Mater. Constr., Woodhead Publishing,
576 2017: pp. 37–60. doi:10.1016/B978-0-08-102009-8.00004-9.

577 [24] Council of the European Union, Council directive 2013/59/EURATOM, European Basic
578 Safety Standards (BSS) for Protection against Ionising Radiation, Off. J. Eur. Union. L
579 13/1 (2014).

580 [25] International Agency for Research on Cancer (IARC), IARC monographs on the
581 identification of carcinogenic hazards to humans, List Classif. Agents Classif. by IARC
582 Monogr. Vol. 1-124. (2019). https://monographs.iarc.fr/list-of-classifications.

583 [26] Y. Ishimori, K. Lange, P. Martin, Y.S. Mayya, M. Phaneuf, Technical Reports Series
584 No. 474: Measurement and Calculation of Radon Releases from NORM Residues,
585 Vienna, 2013.

586 [27] K. Gijbels, R. Ion Iacobescu, Y. Pontikes, N. Vandevenne, S. Schreurs, W.
587 Schroeyers, Radon immobilization potential of alkali-activated materials containing
588 ground granulated blast furnace slag and phosphogypsum, Constr. Build. Mater. 184
589 (2018) 68–75. doi:10.1016/j.conbuildmat.2018.06.162.

590 [28] Q. Zhou, N.B. Milestone, M. Hayes, An alternative to Portland Cement for waste
591 encapsulation-The calcium sulfoaluminate cement system, J. Hazard. Mater. 136
592 (2006) 120–129. doi:10.1016/j.jhazmat.2005.11.038.

593 [29] M.L.D. Gougar, B.E. Scheetz, D.M. Roy, Ettringite and C-S-H portland cement phases
594 for waste ion immobilization: A review, Waste Manag. 16 (1996) 295–303.
595 doi:10.1016/S0956-053X(96)00072-4.

[30] V. Albino, R. Cioffi, M. Marroccoli, L. Santoro, Potential application of ettringite generating systems for hazardous waste stabilization, J. Hazard. Mater. 51 (1996) 241–252. doi:10.1016/S0304-3894(96)01828-6.

[31] O. Hjelmar, M. Wahlström, R. Comans, U. Kalbe, P. Grathwohl, J. Mehu, N. Schiopu, J. Hykš, J. Laine-ylijoki, A. van Zomeren, O. Krüger, U. Schoknecht, T. Wendel, M. Abdelghafour, N. Borho, Robustness validation of two harmonized European leaching tests for assessment of the leaching of construction products, including waste-based construction materials, in: WASCON 2012 Gothenburg, Sweden, 2012: pp. 1–5.

[32] European Committee for Standardization, CEN/TC 351. Construction Products: Assessment of release of dangerous substances, (2014).

[33] European Committee for Standardization, CEN/TS 16637-3. Construction products: Assessment of release of dangerous substances - Part 3: Horizontal up-flow percolation test, (2016).

[34] K. Gijbels, H. Nguyen, P. Kinnunen, W. Schroeyers, Y. Pontikes, S. Schreurs, M. Illikainen, Feasibility of incorporating phosphogypsum in ettringite-based binder from ladle slag, J. Clean. Prod. 237 (2019) 117793. doi:10.1016/j.jclepro.2019.117793.

[35] European Committee for Standardization, EN 450-1: Fly ash for concrete - Part 1: Definition, specifications and conformity criteria, (2012).

[36] A. Shakhashiro, U. Sansone, H. Wershofen, A. Bollhöfer, C.K. Kim, C.S. Kim, G. Kis-Benedek, M. Korun, M. Moune, S.H. Lee, S. Tarjan, M.S. Al-Masri, The new IAEA reference material: IAEA-434 technologically enhanced naturally occurring radioactive materials (TENORM) in phosphogypsum, Appl. Radiat. Isot. 69 (2011) 231–236. doi:10.1016/j.apradiso.2010.09.002.

[37] L. Lutterotti, S. Matthies, H.R. Wenk, MAUD (Material Analysis Using Diffraction): a user friendly java program for Rietveld texture analysis and more, in: Jerzy A. Szpunar (Ed.), Proc. Twelfth Int. Conf. Textures Mater. / ICOTOM-12, National Research Press, Montreal, 1999: p. 1599.

[38] H.M. Rietveld, A profile refinement method for nuclear and magnetic structures, J. Appl. Crystallogr. 2 (1969) 65–71. doi:10.1107/S0021889869006558.

[39] B. Michalik, G. de With, W. Schroeyers, Measurement of radioactivity in building materials - Problems encountered caused by possible disequilibrium in natural decay series, Constr. Build. Mater. 168 (2018) 995–1002. doi:10.1016/j.conbuildmat.2018.02.044.

[40] Laboratoire National Henri Becquerel (LNHB), Decay Data Evaluation Project, (n.d.). http://www.nucleide.org/DDEP.htm.

[41] European Committee for Standardization, EN 196-6. Methods of testing cement - Part 6: Determination of fineness, (2010).

[42] OECD (Organization for Economic Cooperation and Development), Exposure to radiation from the natural radioactivity in building materials, Paris, 1979.

[43] J. Somlai, B. Kanyár, R. Bodnár, C. Németh, Z. Lendvai, Radiation dose contribution from coal-slags used as structural building material, J. Radioanal. Nucl. Chem. Artic. 207 (1996) 437–443. doi:10.1007/BF02071248.

[44] C. Nuccetelli, F. Leonardi, R. Trevisi, A new accurate and flexible index to assess the contribution of building materials to indoor gamma exposure, J. Environ. Radioact. 143 (2015) 70–75. doi:10.1016/j.jenvrad.2015.02.011.

[45] T. Croymans, F. Leonardi, R. Trevisi, C. Nuccetelli, S. Schreurs, W. Schroeyers, Gamma exposure from building materials - A dose model with expanded gamma lines

643 from naturally occurring radionuclides applicable in non-standard rooms, Constr. Build.
644 Mater. 159 (2017) 768–778. doi:10.1016/j.conbuildmat.2017.10.051.

645 [46] Z. Sas, J. Szántó, J. Kovács, J. Somlai, T. Kovács, Influencing effect of heat-treatment
646 on radon emanation and exhalation characteristic of red mud, J. Environ. Radioact.
647 148 (2015) 27–32. doi:10.1016/J.JENVRAD.2015.06.002.

648 [47] K. Kovler, A. Perevalov, V. Steiner, L.A. Metzger, Radon exhalation of cementitious
649 materials made with coal fly ash: Part 1 - Scientific background and testing of the
650 cement and fly ash emanation, J. Environ. Radioact. 82 (2005) 321–334.
651 doi:10.1016/j.jenvrad.2005.02.004.

652 [48] K. Gijbels, S. Landsberger, P. Samyn, R. Ion Iacobescu, Y. Pontikes, S. Schreurs, W.
653 Schroeyers, Radiological and non-radiological leaching assessment of alkali-activated
654 materials containing ground granulated blast furnace slag and phosphogypsum, Sci.
655 Total Environ. 660 (2019) 1098–1107. doi:10.1016/j.scitotenv.2019.01.089.

656 [49] S. Brunauer, P.H. Emmett, E. Teller, Adsorption of gases in multimolecular layers, J.
657 Am. Chem. Soc. 60 (1938) 309–319. doi:10.1021/ja01269a023.

658 [50] E.P. Barrett, L.G. Joyner, P.P. Halenda, The determination of pore volume and area
659 distributions in porous substances. I. Computations from nitrogen isotherms, J. Am.
660 Ceram. Soc. 73 (1951) 373–380.

661 [51] B.C. Lippens, J.H. de Boer, Studies on pore systems in catalysts: V. The t method, J.
662 Catal. 4 (1965) 319–323. doi:10.1016/0021-9517(65)90307-6.

663 [52] European Commission, Radiological protection principles concerning the natural
664 radioactivity of building materials - Radiation Protection 112, Luxemburg, 1999.
665 https://ec.europa.eu/energy/sites/ener/files/documents/112.pdf.

666 [53] J.P. Bolivar, R. García-Tenorio, M. García-León, On the fractionation of natural
667 radioactivity in the production of phosphoric acid by the wet acid method, J. Radioanal.
668 Nucl. Chem. Lett. 214 (1996) 77–88. doi:10.1007/BF02164808.

669 [54] W. Schroeyers, Z. Sas, G. Bator, R. Trevisi, C. Nuccetelli, F. Leonardi, S. Schreurs, T.
670 Kovacs, The NORM4Building database, a tool for radiological assessment when using
671 by-products in building materials, Constr. Build. Mater. 159 (2018) 755–767.
672 doi:10.1016/j.conbuildmat.2017.11.037.

673 [55] S.C. Taylor-Lange, M.C.G. Juenger, J.A. Siegel, Radon emanation fractions from
674 concretes containing fly ash and metakaolin, Sci. Total Environ. 466–467 (2014)
675 1060–1065. doi:10.1016/j.scitotenv.2013.08.005.

676 [56] P. de Jong, W. van Dijk, The effect of the composition and production process of
677 concrete on the 222Rn exhalation rate, Environ. Int. 22 (1996) 287–293.
678 doi:10.1016/S0160-4120(96)00120-1.

679 [57] J.G. Ackers, J.F. Den Boer, P. De Jong, R.A. Wolschrijn, Radioactivity and radon
680 exhalation rates of building materials in The Netherlands, Sci. Total Environ. 45 (1985)
681 151–156. doi:10.1016/0048-9697(85)90215-3.

682 [58] K. Kovler, Does the utilization of coal fly ash in concrete construction present a
683 radiation hazard?, Constr. Build. Mater. 29 (2012) 158–166.
684 doi:10.1016/j.conbuildmat.2011.10.023.

685 [59] Z. Sas, W. Sha, M. Soutsos, R. Doherty, D. Bondar, K. Gijbels, W. Schroeyers,
686 Radiological characterisation of alkali-activated construction materials containing red
687 mud, fly ash and ground granulated blast-furnace slag, Sci. Total Environ. 659 (2019)
688 1496–1504. doi:10.1016/j.scitotenv.2019.01.006.

689 [60] W. Zhang, Y. Zhang, Q. Sun, Analyses of influencing factors for radon emanation and

690 exhalation in soil, Water. Air. Soil Pollut. 230 (2019). doi:10.1007/s11270-018-4063-z.

691 [61] K. Kovler, Mechanisms of radon exhalation from hardening cementitious materials,
692 ACI Mater. J. 105 (2008) 404–413.

693 [62] J.E. Rossen, K.L. Scrivener, Optimization of SEM-EDS to determine the C–A–S–H
694 composition in matured cement paste samples, Mater. Charact. 123 (2017) 294–306.
695 doi:10.1016/j.matchar.2016.11.041.

696 [63] D. Herfort, D.E. Macphee, Components in Portland cement clinker and their phase
697 relationships, in: P.C. Hewlett, M. Liska (Eds.), Lea's Chem. Cem. Concr., 5th ed.,
698 Butterworth-Heinemann, 2019: pp. 57–86. doi:10.1016/B978-0-08-100773-0.00003-4.

699 [64] L. Kriskova, Y. Pontikes, Ö. Cizer, G. Mertens, W. Veulemans, D. Geysen, P.T. Jones,
700 L. Vandewalle, K. Van Balen, B. Blanpain, Effect of mechanical activation on the
701 hydraulic properties of stainless steel slags, Cem. Concr. Res. 42 (2012) 778–788.
702 doi:10.1016/j.cemconres.2012.02.016.

703 [65] Y. Jeong, C.W. Hargis, S.C. Chun, J. Moon, The effect of water and gypsum content
704 on strätlingite formation in calcium sulfoaluminate-belite cement pastes, Constr. Build.
705 Mater. 166 (2018) 712–722. doi:10.1016/j.conbuildmat.2018.01.153.

706 [66] B. Lothenbach, D.A. Kulik, T. Matschei, M. Balonis, L. Baquerizo, B. Dilnesa, G.D.
707 Miron, R.J. Myers, Cemdata18: A chemical thermodynamic database for hydrated
708 Portland cements and alkali-activated materials, Cem. Concr. Res. 115 (2019) 472–
709 506. doi:10.1016/j.cemconres.2018.04.018.

710 [67] R.B. Perkins, C.D. Palmer, Solubility of ettringite (Ca6[Al(OH)6]2(SO4)326H2O) at 5–
711 75°C, Geochim. Cosmochim. Acta. 63 (1999) 1969–1980. doi:10.1016/S0016-
712 7037(99)00078-2.

713 [68] W.A. Klemm, J.I. Bhatty, Fixation of heavy metals as oxyanion-substituted ettringites,
714 Skokie, Illinois, USA, 2002.

715 [69] I. Fernández-Olmo, C. Lasa, M.A. Lavín, A. Irabien, Modeling of amphoteric heavy
716 metals solubility in stabilized/solidified steel foundry dust, Environ. Eng. Sci. 26 (2008)
717 251–262. doi:10.1089/ees.2007.0226.

718 [70] S. Peysson, J. Péra, M. Chabannet, Immobilization of heavy metals by calcium
719 sulfoaluminate cement, Cem. Concr. Res. 35 (2005) 2261–2270.
720 doi:10.1016/j.cemconres.2005.03.015.

721 [71] R. Berardi, R. Cioffi, L. Santoro, Matrix stability and leaching behaviour in ettringite-
722 based stabilization systems doped with heavy metals, Waste Manag. 17 (1997) 535–
723 540. doi:10.1016/S0956-053X(97)10061-7.

724 [72] M. Chrysochoou, D. Dermatas, Evaluation of ettringite and hydrocalumite formation for
725 heavy metal immobilization: Literature review and experimental study, J. Hazard.
726 Mater. 136 (2006) 20–33. doi:10.1016/j.jhazmat.2005.11.008.

727 [73] H.A. Van der Sloot, Characterization of the leaching behaviour of concrete mortars
728 and of cement-stabilized wastes with different waste loading for long term
729 environmental assessment, Waste Manag. 22 (2002) 181–186. doi:10.1016/S0956-
730 053X(01)00067-8.

731 [74] B.I. Silveira, A.E.M. Dantas, J.E.M. Blasques, R.K.P. Santos, Effectiveness of cement-
732 based systems for stabilization and solidification of spent pot liner inorganic fraction, J.
733 Hazard. Mater. 98 (2003) 183–190. doi:10.1016/S0304-3894(02)00317-5.

734 [75] J.Y. Park, H.J. Byun, W.H. Choi, W.H. Kang, Cement paste column for simultaneous
735 removal of fluoride, phosphate, and nitrate in acidic wastewater, Chemosphere. 70
736 (2008) 1429–1437. doi:10.1016/j.chemosphere.2007.09.012.

[76] A.F.S. Gomes, D.L. Lopez, A.C.Q. Ladeira, Characterization and assessment of chemical modifications of metal-bearing sludges arising from unsuitable disposal, J. Hazard. Mater. 199–200 (2012) 418–425. doi:10.1016/j.jhazmat.2011.11.039.

[77] H. He, H. Suito, Immobilization of fluorine in aqueous solution by calcium aluminum ferrite and the mixture of calcium aluminate and gypsum, ISIJ Int. 42 (2008) 794–799. doi:10.2355/isijinternational.42.794.

[78] Council of the European Union, European drinking water directive 2013/51/EURATOM, laying down requirements for the protection of the health of the general public with regard to radioactive substances in water intended for human consumption, Off. J. Eur. Union. L 296/12 (2013). http://eur-lex.europa.eu/legal-content/EN/TXT/?uri=CELEX%3A32013L0051.

[79] W. Kurdowski, Cement and concrete chemistry, Springer, Krakow, Poland, 2014. doi:10.1007/978-94-007-7945-7.